Vol. 92 No. 5 pp. 1784–1797 ACTA GEOLOGICA SINICA (English Edition) Oct. 2018

Mineralogical Characteristics of Exsolved Spinel in the Panzhihua V-Ti Magnetite Deposit, Sichuan: Implications for the Mineralization Process

ZHANG Zhibin[1], HUANG Fei[1,*], XING Miaomiao[1], WAN Quan[2], GAO Wenyuan[1], GAO Shang[3], CHEN Zhenyu[4] and CAI Jianhui[4]

1 *College of Resources and Civil Engineering, Northeastern University, Shenyang 110819, China*
2 *State Key Laboratory of Ore Deposit Geochemistry, Institute of Geochemistry, Chinese Academy of Sciences, Guiyang 550081, China*
3 *School of Civil Engineering, Shijiazhuang Tiedao University, Shijiazhuang 050043, China*
4 *Key Laboratory of Metallogeny and Mineral Resource Assesment, Ministry of Land and Resources, Institute of Mineral Resources, Chinese Academy of Geological Sciences, Beijing 100037, China*

Abstract: Spinel exsolution is widespread in titanomagnetite from the Fe-Ti oxide gabbro of the Panzhihua intrusion, Emeishan Large Igneous Province, SW China. However, little research has been conducted into the implications of patterns in the mineralogical characteristics of the spinel for spatial variation in the controls on the exsolution mechanism and, hence, the formation process of the ore deposit. This study selected the Lanjiahuoshan Ore Block in the Panzhihua V-Ti magnetite deposit to explore this issue, systematically studying exsolution textures in the titanomagnetite through petrographic observation and the integrated use of in-situ microanalysis. The results show that the exsolved spinel gradually becomes finer-grained and less abundant from the center to edge and the bottom to top of the ore bodies. Compositionally, there is an inverse correlation between the size of exsolved spinel grains and their Mg# value. In addition, there is compositional zonation in the spinel interiors, with a gradual increase in the Mg content and decrease in Fe content from the core to the rim. The analysis suggests that fractional crystallization of ferrotitanium magma with a high oxygen fugacity in a shallow magma chamber caused compositional differences in the primary magnetite solid solution in different parts of the Panzhihua intrusion. Additionally, the thermal evolution of the magnetite solid solution differed in different parts of orebody, bringing about variations in spinel development. Together, these effects resulted in spatial variation in the abundance, grain size, and morphology of spinel in different parts of the orebody and intrusion that follows an identifiable distribution law. Furthermore, the compositional zonation of exsolved spinels reflects the rapid growth of exsolution features in a high-temperature environment. Thus, the size, morphology, abundance, and composition of spinel exsolution features in titanomagnetite provide a valuable petrogenetic tool for estimating the maturity and formational environment of the deposit.

Key words: spinel exsolution, mineralogical characteristics, compositional zonation, mineralization process, Panzhihua, Sichuan

1 Introduction

The Panzhihua V-Ti magnetite deposit occurring in the Panzhihua mafic layered intrusion, Panzhihua-Xichang, Sichuan province, China is typical of magmatic ore deposits worldwide. Considerable research has been conducted into the geological setting of the rock mass and its petrological, mineralogical, and geochemical characteristics, resulting in a series of findings regarding the deposit genesis and age of ore formation (Song Xieyan et al., 1999, 2001; Lo et al., 2002; Zhou et al., 2002; Hou Zengqian et al., 2005; Ai Yu et al., 2006; Zhong and Zhu, 2006; Pang et al., 2009; Zhang et al., 2009; Zhang Xiaoqi et al., 2011; Hou et al., 2011, 2012; Wang Shixia et al., 2012; Hou et al., 2012, 2013; Song et al., 2013). In recent years, many researchers have drawn broad conclusions about the composition and genesis of the magnetite and

* Corresponding author. E-mail: zzbin0502@163.com

ilmenite in this deposit but have not arrived at a consensus on the genesis and magmatic evolution of the magnetite deposit as a whole (Pang et al., 2008, 2009; Song et al., 2013; She Yuwei et al., 2014; Zheng Wenqin et al., 2014).

Spinel, a common mineral in igneous and metamorphic rocks in the Earth's crust and upper mantle, is sensitive to changes in physicochemical conditions. Spinel is often used as a key indicator of the formational environment and tectonic background of the rocks within which it occurs, because the chemical constitution of spinel and the mineral assemblage it occurs within not only reveal the physicochemical conditions of its formation but can also provide constraints for petrological and geodynamic inferences (Irvine, 1967; Barnes and Roeder, 2001; Ahmed et al., 2005; Karipi et al., 2007; Guo Guolin et al., 2011; Zeng Linggao et al., 2013; Liu Zhao and Tong Laixi, 2015; Niu Xiaolu et al., 2015; El Dien et al., 2016; Taghipour and Ahmadnejad, 2018).

Titanomagnetite in the Fe-Ti oxide gabbro of the Panzhihua intrusion contains abundant spinel with a variety of morphologies and structures that appears to have formed through exsolution during cooling (Li Wenchen, 1992; Howarth et al., 2013; Liu et al., 2015; Zhang Zhibin et al., 2018). Mineral exsolution can be viewed as a relic of mineralization: not only it is a self-organization phenomenon of the internal structure of a mineral but it also carries information regarding the evolution of the geological environment. The structure, morphology, and chemical composition of exsolution features can reflect the formation and evolutionary history of the overall rock (Sautter et al., 1991; Luo et al., 2001; Sun et al., 2007; Zhu Yongfeng and Massonne, 2007; Zhu Yongfeng and Xu Xin, 2007; Yamamoto, 2009; He et al., 2013; Xia Bin et al., 2013; Airiyants et al., 2014; Xu et al., 2015; Guo Guolin et al., 2015; Xiong Fahui et al., 2015, 2016; Zhang Cong et al., 2016), and the thermodynamic behaviors of the solid-solution mineral provide strong indications of both the cooling rate (Rajesh, 2006; McCallum et al., 2006; Yuguchi and Nishiyama, 2007; Ghiorso and Evans, 2008; Righter et al., 2012) and the changes in temperature and pressure (Wang et al., 2005; Adachi et al., 2010).

Currently, systematically gathered compositional data for spinels in the Fe-Ti oxide gabbro in this region are scarce. Although the mineralogical characteristics and exsolution mechanism of the spinel have been described and discussed at length (Wang Yanguo, 1990; Howarth et al., 2013; Liu et al., 2015; Zhang Zhibin et al., 2018), the laws governing the differences in its morphology, grain size and chemical composition, the mechanisms resulting in those laws, and the dynamics of exsolution feature growth are as yet unresolved. On the basis of field investigation, this study selected spinel exsolution in Panzhihua V-Ti magnetite deposits as an appropriate research object to investigate the factors controlling spinel development and to provide a basis for studying the mineralization process of the ore deposit.

2 Geological Setting

The Panzhihua V-Ti magnetite deposit lies in the Panzhihua fault zone at the center of the Emeishan Large Igneous Province. The area is structurally dominated by a sequence of NS-trending faults, along which there has been frequent, intense crustal motion with associated magmatism (Fig. 1). Therefore, the region features abundant volcanic and intrusive rock; the volcanic rocks are mainly Permian Emeishan formation basalts, and the intrusive rocks are generally acidic.

The deposits that occur in the gabbroic body are called the Zhujiabaobao, Lanjahuoshan, Jianbaobao, Daomakan, Gongshan, and Nalaqing from northeast to southwest (Fig. 2). The ore-bearing rock is alternately leucocratic and hypermelanic and is characterized by a typical layering structure and rhythmic texture. The Panzhihua intrusion has been stratigraphically divided into four zones: the Upper Zone , Middle Zone, Lower Zoneand Marginal Zone, and nine ore bodies, numbered I, II, III, IV, IV, V, VI, VII, VII, VIII and IX from the top down. Due to having a higher ore grade and greater ore thickness than the other bodies, the LZ, comprised of the VII and VIII ore bodies, is the main ore-bearing zone. The samples for this study were collected from the VIII ore body in the Lanjahuoshan ore block.

3 Analytical Methods

The quantitative chemical data for spinel were obtained with a JEO-JXA 8230 electron microprobe (EPMA) installed at the Institute of Mineral Resources at the Chinese Academy of Geological Sciences. It was operated with an accelerating voltage of 15 kV, a beam current of 10 nA and a beam size of 5 μm. Natural and synthetic materials were used as standards, and all of the standards were tested for homogeneity before their utilization for the quantitative analysis. The ZAF correction program supplied by the manufacturer was used to carry out matrix corrections.

To identify mineral assemblages and textural relationships, polished sections were studied by optical microscopy under transmitted and reflected light and by field emission scanning electron microscope (FE-SEM). Secondary electron (SE) images, back-scattered electron (BSE) images, and energy dispersive X-ray (EDX) semi-

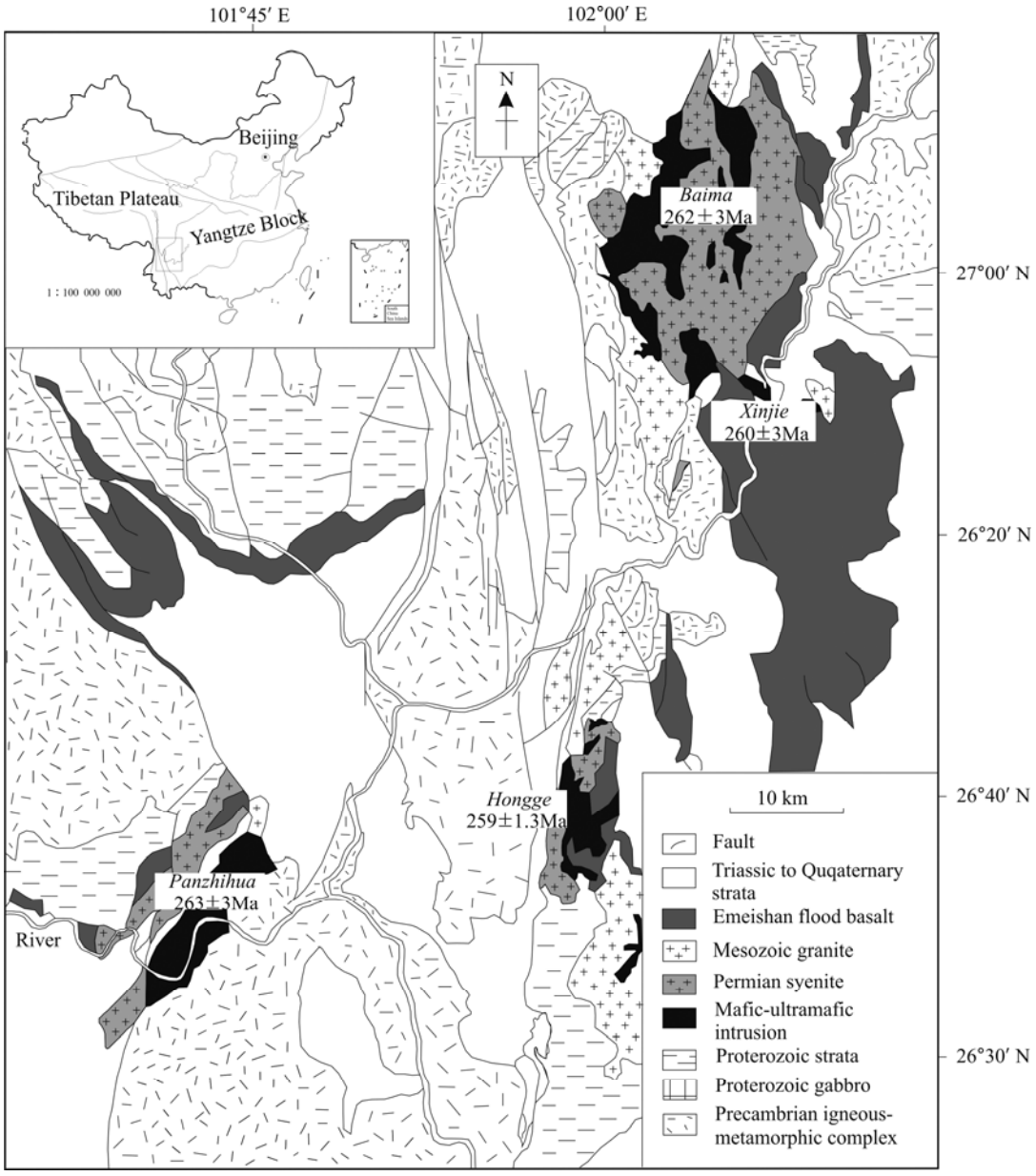

Fig. 1. Generalized geological map of the Pan-Xi area, Emeishan Large Igneous Province, SW China showing the distribution of mafic-ultramafic intrusions (black) that host Fe-Ti oxide mineralization (after Pang et al., 2008). Inset: regional context within China. China basemap after China National Bureau of Surveying and Mapping Geographical Information.

quantitative spectra were taken with an Ultra Plus FE-SEM operating at 20 keV at Northeastern University (Shenyang, China).

4 Results

4.1 Sample location and petrography

Sampling of the VIII orebody was carried out in the Lanjiahuoshan block. The samples are black-gray in hand specimen. There is a gradual reduction in the Fe-Ti oxide content and increase in silicate gangue minerals and metal sulfides from the bottom to the top of the VIII ore body. Samples from the bottom of the VIII orebody are generally dense massive or dense disseminated tectonic, with a granular mosaic structure and minor occurrences of sideronitic texture (Fig. 3a–b). In the upper orebody, there is a gradual change to a sparsely scattered disseminated structure and sideronitic texture (Fig. 3c–d).

The ores are composed mainly of Fe-Ti oxide minerals such as titanomagnetite, magnetite, ilmenite and magnesia-alumina spinel and metal sulfides such as pyrrhotite, chalcopyrite, and pyrite. The gangue minerals are mainly silicates, with a small amount of phosphate and carbonate minerals. Automorphic and hypidiomorphic pyroxene and plagioclase exhibit an irregular arrangement in an almost granular gabbroic texture. Spinel forms a complex

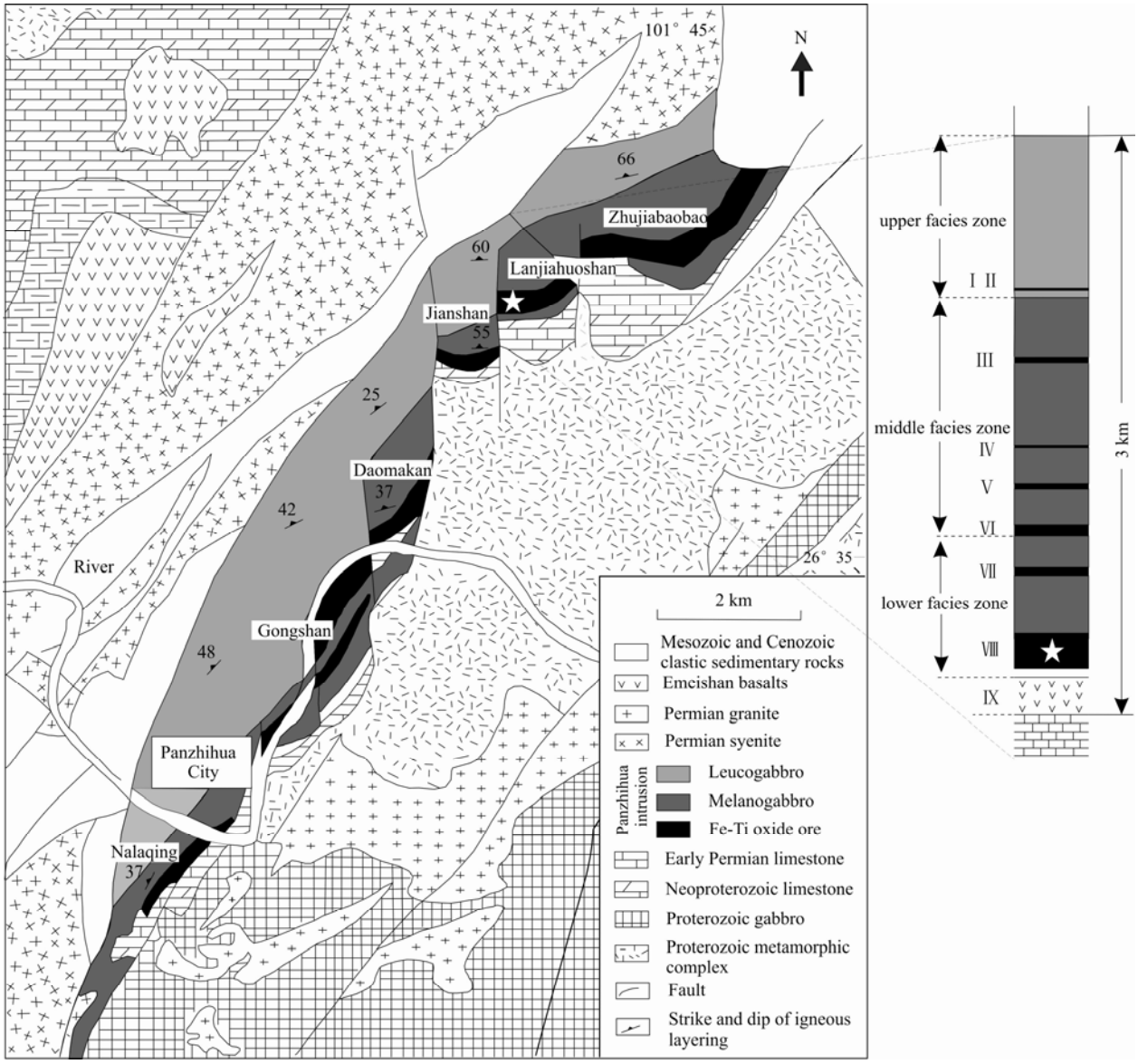

Fig. 2. Geological map of the Panzhihua intrusion, SW China (modified from Pang et al., 2008).

exsolution texture with ilmenite throughout the titanomagnetite.

4.2 Mineralogical characteristics of spinel

4.2.1 Morphology, size, and abundance

Two types of spinel are observed in the titanomagnetite: granular exsolution with a grain size in the range 200 nm–80 μm (Fig. 4a) and lamellae parallel to {100} in the titanomagnetite, about 100 nm–5 μm long and 5–60 μm wide (Fig. 4b).

Spinel morphology, grain size, and abundance differ significantly in different parts of the ore body and in different types of ore and follow an identifiable change law. Spinel exsolution occurs in greater abundance and is coarser-grained in the middle of the ore body than at the margins (Li Wenchen, 1992). Spinel exsolution features at the bottom of the VIII orebody are generally larger, with a euhedral-granular form (Fig. 5a–c) and often form complicated polygonal exsolution patterns with surrounding smaller spinels (Fig. 5d). Spinel exsolution in the upper part of orebody often occurs as an emulsion texture, spindly texture or as lamellae (Fig. 5e–g). There are fewer exsolved spinels at the top of the orebody than in the other parts of the orebody (Fig. 5h–i). Overall, the distribution of spinel exsolution is relatively uniform, with a directional arrangement.

4.2.2 Compositions

Surface scanning analysis showed that the main elements within the spinel exsolution are Al and Mg (Fig. 6b–c). The symbiotic exsolved ilmenites form a fenestral fabric composed of Ti and Fe (Fig. 6d–e). Chemical

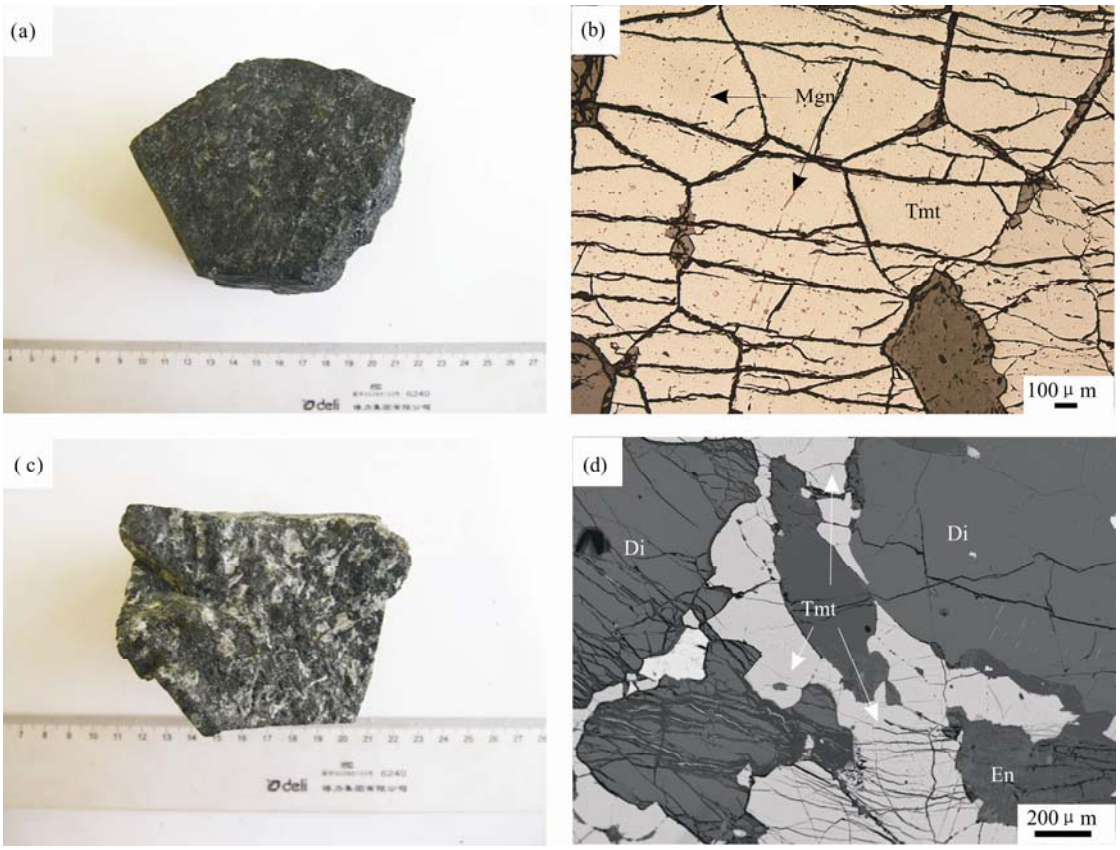

Fig. 3. Textures and structure in rocks of the Panzhihua deposit.
(a), Dense massive structure ore; (b), granular mosaic structure of titanomagnetite, the granular spinel exsolutions scatteredly distribute in the titanomagnetite; (c), dense disseminated structure ore; (d), sideronitic texture, titanomagnetites occur between the gangue minerals as xenomorphic granular (BSE image). Di=Diopside; En=Enstatite; Mgn= magnesia-alumina spinel ; Tmt=titanomagnetite.

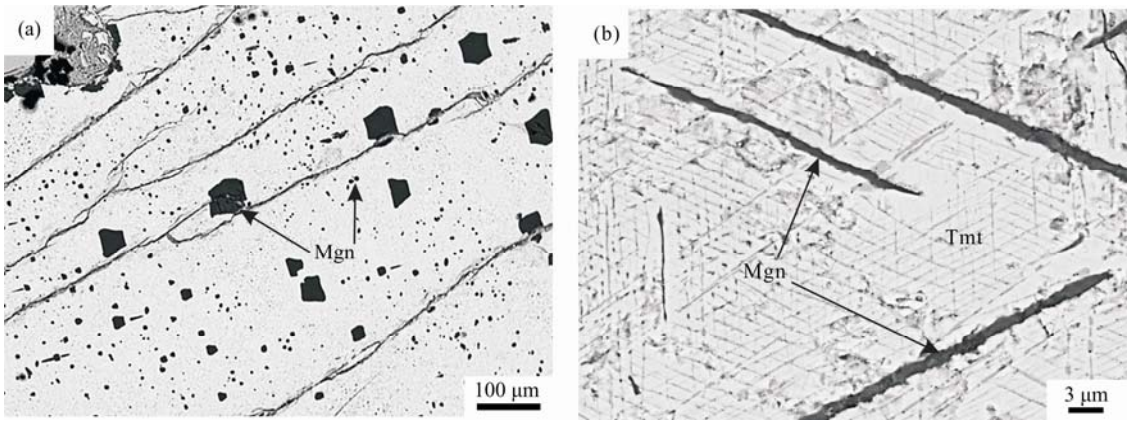

Fig. 4. The morphology of magnesia-alumina spinel exsolution.
(a), The granular spinel exsolution with big grain size (200nm-80μm) and euhedral crystal; (b), the spinel lamellae parallel to the {100} of the titanomagnetite.

composition analysis by electron microprobe confirms that the titanomagnetite is composed of magnetite with spinel and ilmenite exsolution (Tables 1–3). The chemical composition of the spinel is between magnesium spinel and hercynite spinel, with an $Mg^{\#}$ [=100×Mg/(Mg+Fe^{2+})] of 77–81 and $Cr^{\#}$ [=100×Cr/(Cr+Al)] below 0.1. The exsolved spinel in the Panzhihua Fe-Ti oxide deposits is magnesia-alumina spinel under the classification of spinellides according to their $Cr^{\#}$ (Carswell, 1980).

The larger the spinel grain size, the smaller its $Mg^{\#}$ (Table 1). Furthermore, compositional zonation is seen in the spinel interiors, with Mg increasing and Fe reducing gradually from core to rim. This zonation differs by grain size, with coarser-grained spinels having more obvious differences in the Mg-Fe component than finer-grained spinels (Fig. 7).

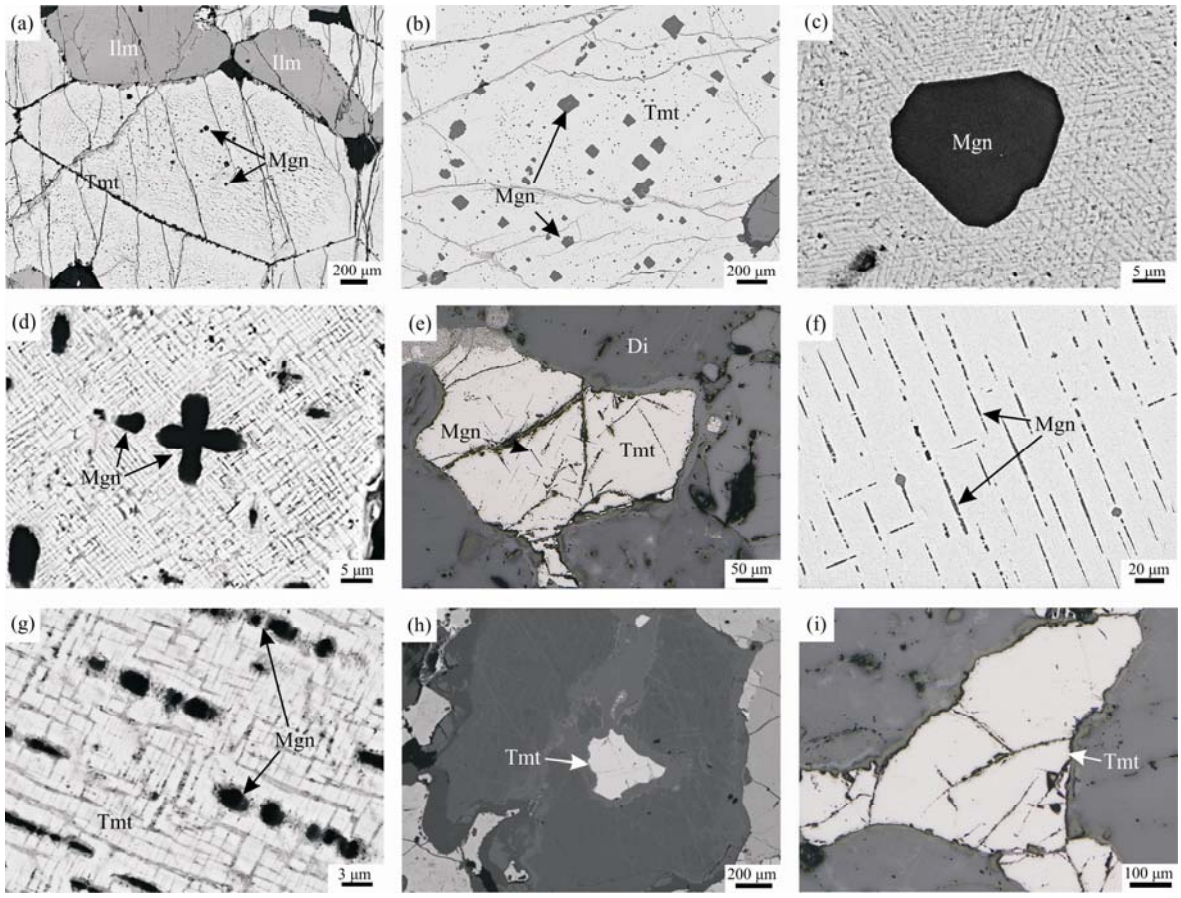

Fig. 5. Microphotographs and backscatter electron images (BSE images) of spinel exsolution in different parts of the ore body.
(a–b), Large granular exsolved spinels distributed in the titanomagnetite in dense massive tectonic ore; (c), granular exsolved spinel with a euhedral-granular texture; (d), large exsolved spinels form complicated polygonal exsolution features with surrounding smaller spinels; (e–g), spinel exsolution lamellae in titanomagnetite in disseminated tectonic ore; (h–i), Titanomagnetite with scarce spinel exsolution in sparsely scattered disseminated tectonic ore. Di=diopside; Ilm=Ilmenite; Tmt=titanomagnetite;Mgn= magnesia-alumina spinel.

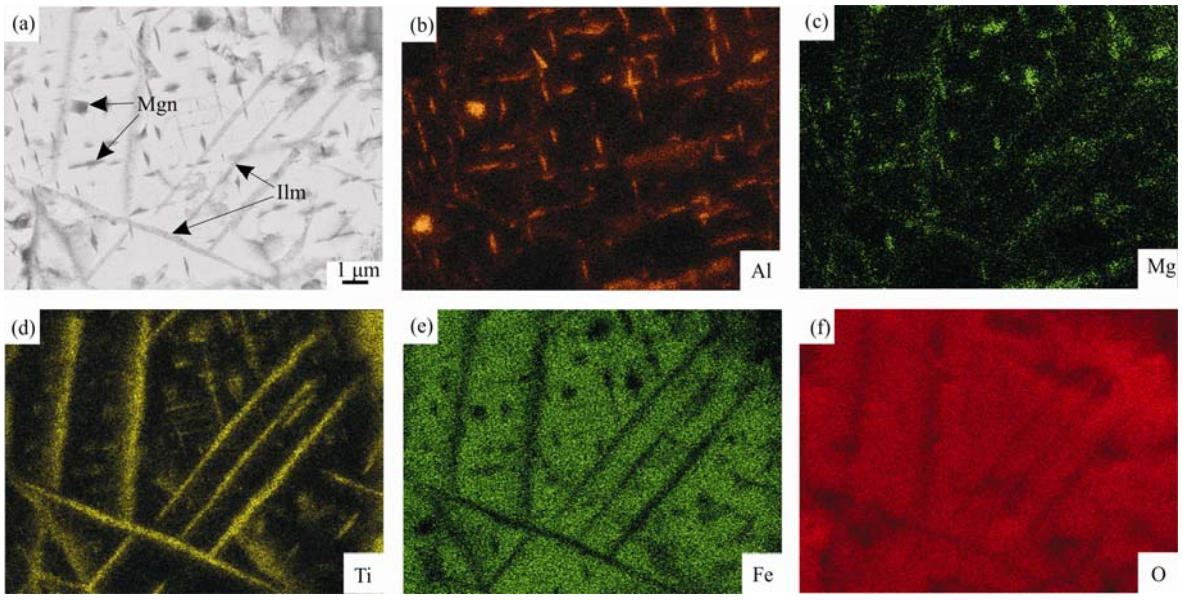

Fig. 6. BSE image and map analyses with SEM of the exsolution texture in titanomagnetite.
Ilm=Ilmenite; Mgn= magnesia-alumina spinel

Table 1 EPMA data for exsolved spinels of different granularity

No	1	2	3	4	5	6	7	8	9	10	11	12
Na_2O(wt%)	0.04	0.03	0.04	0.03	0.02	0.04	0.05	0.05	0.00	0.05	0.06	0.04
MgO	21.31	21.53	20.76	21.36	21.11	21.30	21.78	21.54	21.35	21.18	21.52	20.82
Al_2O_3	65.83	65.72	64.54	65.66	65.36	65.52	66.47	66.60	65.63	66.22	66.78	66.12
SiO_2	0.18	0.13	0.15	0.011	0.17	0.14	0.10	0.13	0.13	0.14	0.04	0.12
BaO	0.07	0.04	0.00	0.02	0.03	0.04	0.00	0.00	0.02	0.00	0.00	0.00
FeO	10.54	9.47	10.63	9.88	10.19	9.82	9.70	9.90	10.22	10.70	10.02	10.87
Fe_2O_3	1.73	1.61	3.18	2.93	2.77	2.46	2.43	1.62	2.58	2.73	1.48	2.18
MnO	0.08	0.06	0.07	0.01	0.08	0.06	0.05	0.02	0.04	0.07	0.04	0.01
NiO	0.00	0.05	0.00	0.03	0.05	0.00	0.00	0.03	0.00	0.00	0.00	0.03
TiO_2	0.66	0.44	0.24	0.18	0.21	0.25	0.32	0.38	0.31	0.26	0.47	0.21
Cr_2O_3	0.09	0.07	0.08	0.07	0.08	0.06	0.08	0.06	0.09	0.07	0.11	0.05
V_2O_3	0.13	0.07	0.04	0.01	0.05	0.03	0.11	0.08	0.08	0.12	0.13	0.10
Total	100.66	99.22	99.75	100.31	100.14	99.73	101.11	100.41	100.47	101.55	100.68	100.62
Na *apfu*	0.002	0.001	0.002	0.001	0.001	0.002	0.002	0.003	0.000	0.002	0.003	0.002
Mg	0.791	0.806	0.781	0.795	0.789	0.797	0.802	0.798	0.794	0.781	0.795	0.774
Al	1.932	1.946	1.920	1.933	1.931	1.937	1.936	1.950	1.930	1.931	1.951	1.944
Si	0.004	0.003	0.004	0.003	0.004	0.004	0.003	0.003	0.003	0.004	0.001	0.003
Ba	0.001	0.000	0.000	0.000	0.000	0.000	0.000	0.000	0.000	0.000	0.000	0.000
Fe^{2+}	0.219	0.199	0.225	0.207	0.214	0.206	0.201	0.206	0.213	0.221	0.208	0.227
Fe^{3+}	0.032	0.030	0.060	0.055	0.052	0.046	0.045	0.030	0.048	0.051	0.028	0.041
Mn	0.002	0.001	0.001	0.000	0.002	0.001	0.001	0.001	0.001	0.001	0.001	0.000
Ni	0.000	0.001	0.000	0.000	0.001	0.000	0.000	0.001	0.000	0.000	0.000	0.001
Ti	0.012	0.008	0.005	0.003	0.004	0.005	0.006	0.007	0.006	0.005	0.009	0.004
Cr	0.002	0.001	0.002	0.002	0.002	0.001	0.002	0.001	0.002	0.001	0.002	0.001
V	0.003	0.001	0.001	0.000	0.001	0.001	0.002	0.002	0.002	0.002	0.003	0.002
$Mg^{\#}$	78.28	80.22	77.68	79.39	78.70	79.45	80.00	79.51	78.83	77.92	79.29	77.34
$Cr^{\#}$	0.09	0.07	0.08	0.08	0.08	0.06	0.08	0.06	0.09	0.07	0.10	0.05
DIA (μm)	19	14	43	48	39	27	16	20	25	32	11	58

a. $Mg^{\#}$ [=100×Mg/(Mg+Fe^{2+})]; $Cr^{\#}$ [=100×Cr/(Cr+Al)].
b. Redistribution of ΣFeO between Fe_2O_3 and FeO is on the basis of charge balance and stoichiometry of spinel.

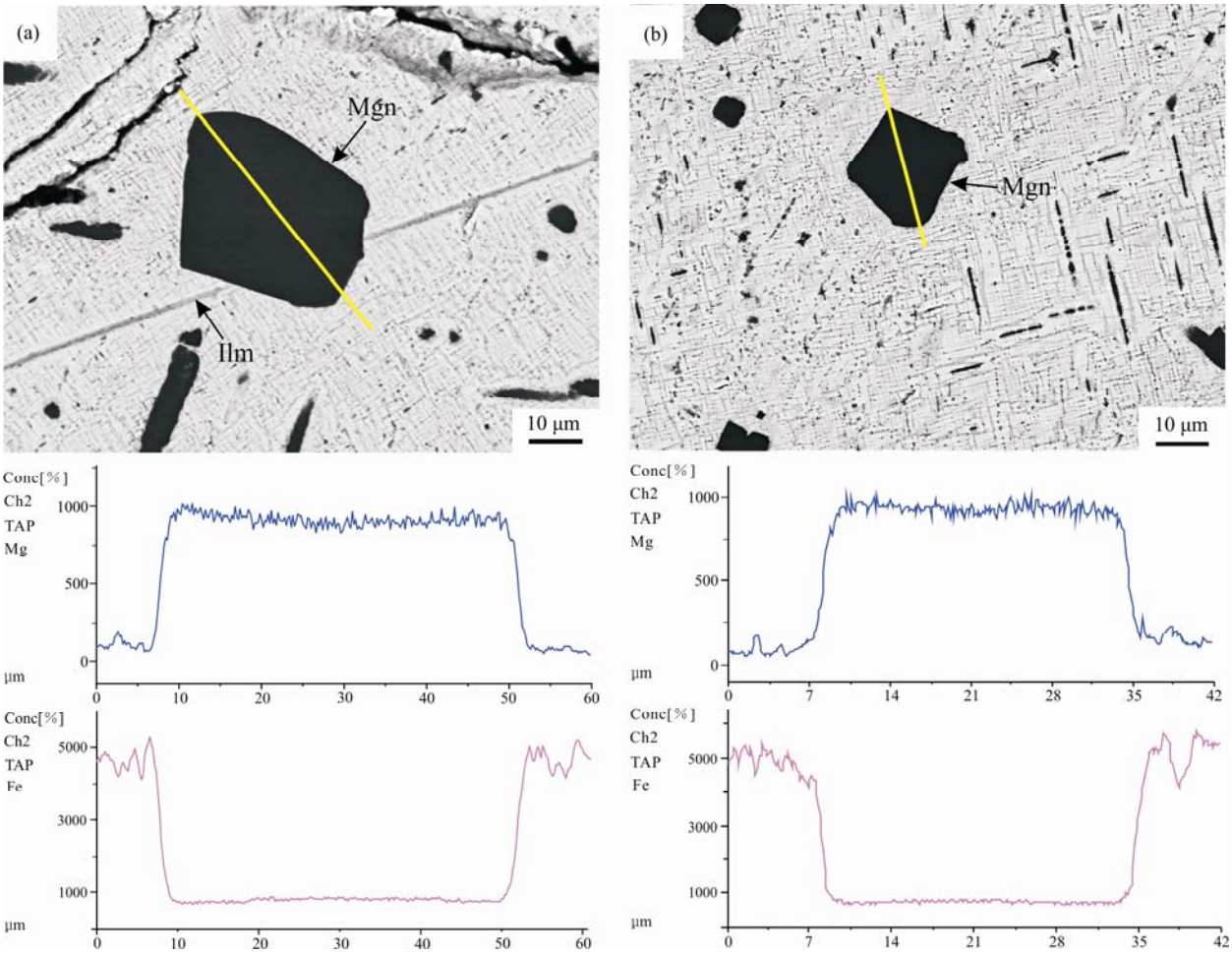

Fig. 7. Cross-sectional profiles obtained by electron probe microanalysis of exsolved spinel of different grain size.

Table 2 EPMA data for the magnetite in titanomagnetite

No.	1	2	3	4	5	6	7	8	9	10	11	12
Na_2O (wt%)	0.00	0.00	0.00	0.03	0.00	0.00	0.00	0.07	0.00	0.03	0.02	0.00
MgO	2.69	2.45	3.36	2.68	4.72	3.47	2.73	1.85	2.26	3.44	2.25	2.28
Al_2O_3	1.40	1.92	3.00	1.63	6.01	2.35	1.95	2.21	1.90	2.24	2.14	0.86
SiO_2	0.05	0.03	0.07	0.03	0.01	0.02	0.01	0.03	0.01	0.05	0.05	0.03
BaO	0.59	0.56	0.13	0.70	0.00	0.00	0.00	0.05	0.08	0.11	0.47	0.31
FeO	40.53	38.73	35.94	40.50	37.58	41.72	41.10	40.63	40.21	40.08	38.43	38.46
Fe_2O_3	40.83	44.22	42.70	41.13	36.51	37.72	41.28	39.82	39.89	38.97	46.94	47.05
MnO	0.16	0.30	0.47	0.23	0.28	0.27	0.33	0.57	0.39	0.39	0.13	0.23
NiO	0.04	0.00	0.85	0.01	0.00	0.00	0.00	0.01	0.00	0.00	0.02	0.01
TiO_2	14.36	12.05	12.56	14.21	14.00	16.19	14.49	13.99	13.97	15.07	10.95	11.37
Cr_2O_3	0.07	0.09	0.10	0.08	0.04	0.00	0.00	0.03	0.06	0.07	0.10	0.06
V_2O_3	0.93	1.33	0.90	1.28	0.60	0.78	0.57	0.48	0.39	0.77	0.99	1.24
P_2O_5	0.02	0.00	0.00	0.00	0.03	0.00	0.00	0.00	0.00	0.03	0.00	0.00
Total	101.68	101.68	100.10	102.33	99.79	102.52	102.45	99.75	99.16	101.25	102.48	101.90
Na *apfu*	0.000	0.000	0.000	0.002	0.000	0.000	0.000	0.005	0.000	0.002	0.002	0.000
Mg	0.146	0.133	0.183	0.144	0.250	0.184	0.146	0.102	0.125	0.185	0.121	0.124
Al	0.060	0.083	0.129	0.070	0.252	0.099	0.083	0.097	0.083	0.095	0.091	0.037
Si	0.002	0.001	0.003	0.001	0.000	0.001	0.000	0.001	0.001	0.002	0.002	0.001
Ba	0.008	0.008	0.002	0.007	0.000	0.000	0.000	0.001	0.001	0.002	0.007	0.004
Fe^{2+}	1.235	1.181	1.097	1.224	1.118	1.242	1.236	1.260	1.253	1.210	1.164	1.178
Fe^{3+}	1.119	1.213	1.173	1.119	0.977	1.010	1.117	1.111	1.119	1.058	1.279	1.296
Mn	0.005	0.009	0.014	0.007	0.008	0.008	0.010	0.018	0.012	0.012	0.004	0.007
Ni	0.001	0.000	0.025	0.000	0.000	0.000	0.000	0.000	0.000	0.000	0.001	0.000
Ti	0.394	0.331	0.345	0.386	0.375	0.434	0.392	0.390	0.392	0.409	0.298	0.313
Cr	0.002	0.003	0.003	0.002	0.001	0.000	0.000	0.001	0.002	0.002	0.003	0.002
V	0.027	0.039	0.026	0.037	0.017	0.022	0.016	0.014	0.012	0.022	0.029	0.036
P	0.001	0.000	0.000	0.000	0.001	0.000	0.000	0.000	0.000	0.001	0.000	0.000

a. Redistribution of ΣFeO between Fe_2O_3 and FeO is on the basis of charge balance and stoichiometry of magnitite.

Table 3 EPMA data for the gangue minerals and associated ilmenite

	Diopside			Forsterite		Anorthite			Ilmenite			
No.	1	2	3	4	5	6	7	8	9	10	11	12
Na_2O(wt%)	0.03	0.02	0.01	0.00	0.00	0.21	0.19	0.22	0.01	0.01	0.04	0.00
K_2O	0.00	0.00	0.00	0.00	0.01	0.04	0.01	0.01	0.00	0.00	0.00	0.00
CaO	23.25	22.73	21.68	0.06	0.02	12.56	13.54	13.22	0.00	0.00	0.00	0.00
MgO	13.92	13.88	13.80	43.28	44.03	0.00	0.02	0.02	8.34	8.29	8.09	3.43
Al_2O_3	4.61	4.81	4.26	0.00	0.01	30.03	30.70	30.14	0.03	0.03	0.02	0.00
SiO_2	50.51	50.26	51.13	41.11	41.43	54.34	53.32	53.75	0.02	0.02	0.00	0.03
BaO	0.05	0.11	0.08	0.02	0.00	0.01	0.01	0.02	1.90	2.30	1.50	1.50
FeO	6.07	6.66	6.83	15.59	15.13	0.17	0.12	0.23	30.49	29.99	31.22	38.35
Fe_2O_3	0.02	0.00	0.00	0.12	0.00	0.00	0.03	0.00	6.91	8.30	6.91	5.86
MnO	0.00	0.16	0.16	0.15	0.12	0.01	0.00	0.05	0.34	0.28	0.33	0.36
NiO	0.02	0.00	0.00	0.11	0.00	0.00	0.00	0.00	0.00	0.00	0.00	0.00
TiO_2	1.67	1.70	1.59	0.01	0.08	0.03	0.00	0.02	51.84	51.31	52.10	50.57
Cr_2O_3	0.02	0.03	0.01	0.00	0.02	0.00	0.00	0.00	0.01	0.02	0.01	0.01
V_2O_3	0.09	0.05	0.14	0.09	0.09	0.09	0.09	0.09	0.72	0.68	0.75	0.77
P_2O_5	0.07	0.02	0.00	0.01	0.03	0.02	0.01	0.02	0.00	0.00	0.01	0.00
Total	100.29	100.44	99.67	100.55	100.98	97.51	98.17	97.78	100.60	101.23	100.98	100.87
Na *apfu*	0.002	0.003	0.001	0.000	0.000	0.018	0.017	0.020	0.001	0.001	0.002	0.000
K	0.000	0.000	0.000	0.000	0.000	0.002	0.001	0.000	0.000	0.000	0.000	0.000
Ca	0.918	0.899	0.860	0.002	0.001	0.613	0.659	0.645	0.000	0.000	0.000	0.000
Mg	0.765	0.764	0.762	1.610	1.625	0.000	0.001	0.001	0.297	0.294	0.287	0.126
Al	0.200	0.209	0.186	0.000	0.000	1.611	1.644	1.619	0.001	0.001	0.000	0.000
Si	1.862	1.855	1.893	1.026	1.025	2.473	2.423	2.449	0.000	0.001	0.000	0.001
Ba	0.001	0.002	0.001	0.000	0.000	0.000	0.000	0.000	0.018	0.021	0.014	0.014
Fe^{2+}	0.187	0.206	0.211	0.325	0.313	0.006	0.005	0.007	0.608	0.597	0.621	0.790
Fe^{3+}	0.001	0.000	0.000	0.002	0.000	0.000	0.001	0.000	0.124	0.149	0.124	0.109
Mn	0.000	0.005	0.005	0.003	0.003	0.001	0.001	0.002	0.007	0.006	0.007	0.007
Ni	0.001	0.000	0.000	0.002	0.000	0.000	0.001	0.000	0.000	0.000	0.000	0.000
Ti	0.046	0.047	0.044	0.000	0.002	0.001	0.002	0.001	0.931	0.918	0.932	0.937
Cr	0.001	0.001	0.000	0.000	0.000	0.000	0.000	0.000	0.000	0.000	0.000	0.000
V	0.003	0.002	0.004	0.002	0.002	0.003	0.003	0.003	0.014	0.013	0.014	0.015
P	0.002	0.001	0.000	0.000	0.001	0.001	0.000	0.001	0.000	0.000	0.000	0.000

a. 1–3: The composition data of diopside; 4–5: the composition data of forsterite; 6–8: the composition data of anorthite; 9–12: the composition data of Ilmenite. b. the atomic proportions are calculated on a basis of oxygen atoms. diopside is normalized to 6, forsterite to 4, anorthite to 8, and ilmenite corundum to 3 oxygens.

5 Discussion

Recent studies have shown that magnetite formed as a homogeneous solid solution in the process of magmatic crystallization. Al, Ti, V, Si, Ca, Mn and Mg are incorporated into the magnetite lattice through isomorphic

substitution. The magnetite solid solution becomes unstable as the temperature decreases and solute elements exsolve from it in the form of new minerals (Shimazaki, 1998; Dare et al., 2012; Nadoll et al., 2012; Hu Hao et al., 2014).

The spinel in the titanomagnetite is the result of this exsolution from the magnetite solid solution during cooling. The differences in the thermal history of the magnetite solid solution during cooling resulted in differences in the development of the spinels, resulting in the observed distribution patterns in the abundance, grain size, and morphology of exsolved spinels within the orebody and intrusion. Therefore, the spinel can provide an important petrogenetic tool for determining the metallogenetic environment and thermal history of the deposit.

5.1 Relationship between morphology, size and abundance of spinel and mineralization process of the deposit

The clear contact between the deposit and the mafic-ultramafic rock shows that metallization to form the Panzhihua V-Ti magnetite deposit occurred through the separation of immiscible phases in the fluid system of the melt. However, the spatial distribution of ore types inside the deposit additionally indicates the action of fractional crystallization. It has been noted previously that the exsolved spinels occur in greater quantities and with coarser grain sizes in the middle of the ore body than at the margin (Li Wenchen, 1992), and this study shows similar changes from top to bottom, with a gradual increase in spinel abundance, grain size, and morphological complexity.

Spinel growth is strongly controlled by the physical and chemical conditions in its formational environment. The massive Fe–Ti oxide ores at the bottom of the Panzhihua intrusions, which were crystallized first, are more enriched in Mg and Al due to the high oxygen fugacities (fO_2) of the parental magmas. As fO_2 decreased with the evolution of magma, silicate mineral crystals will have consumed the Mg and Al, and the ores formed began to have a sideronitic texture and sparse, scattered disseminated structure (Pang et al., 2008; Zhang Xiaoqi et al., 2011; Wang Shixia et al., 2012; Zheng et al., 2014).

Additionally, temperature will have had a controlling influence on spinel development. This is because exsolution occurs through solid diffusion, strongly dependent on temperature following the Arrhenius equation:

$$D = \mathrm{A}e^{-E/(\mathrm{RT})} \quad (1)$$

where A is the pre-exponential factor, E is activation energy, and R is the molar gas constant.

A drop in temperature will reduce the solubility of Mg and Al in the magnetite solid solution; however, according to Equation (1), the ions diffusion rate decreases sharply with a decrease in temperature. Therefore, if the temperature falls sharply, exsolution will not occur (Priece , 1981). In the ore body as a whole, the cooling rate reduced gradually from the edge to center, and the bottom of the orebody has a longer cooling history, a higher temperature of crystallization, and a lower cooling rate than the upper part (Zhang Xiaoqi et al., 2011; Zhang Zhibin et al., 2018).

It is proposed that the correspondence between the mineralogical characteristics of the spinel and the ore types shows that the growth of the spinel has a close relationship with the overall mineralization process of the deposit. At the edge and top of the ore body, the magnetite solid solution has a lower Mg and Al content and the high cooling rate($\triangle T$) will have impeded the diffusion of Mg and Al. Thus, the solute will not have been able to accumulate sufficiently to form exsolution features. The lower cooling rate in the interior of the ore body than at the edge will have been more conducive to spinel exsolution from the magnetite solid solution; however, due to the low temperature, the grains remained small. At the center and bottom of the orebody, the magnetite solid solution has a higher Mg and Al content. This abundance, together with the more rapid diffusion resulting from the higher temperature, facilitated spinel exsolution from the magnetite solid solution through Mg and Al migration (Fig. 8). The slow cooling and high temperature will have also promoted Ostwald ripening. The coarser euhedral-granular spinals absorbed the smaller spinels around them to form complicated polygonal exsolution features.

Therefore, the fractional crystallization of ferrotitanium magma with a high oxygen fugacity in a shallow magma chamber led to a compositional gradient in the primary magnetite solid solution of the Panzhihua intrusion. Additionally, differences in the thermal history of the magnetite solid solution from top to bottom and inside to rim led to differences in the potential for spinel growth. Together, these factors resulted in a clear spatial pattern in the distribution of the abundance, grain size, and morphology of exsolved spinels in different parts of the orebody and intrusion. Coarser-grained exsolved spinels with a more complex morphology indicate that the ore body containing them has a lower cooling rate and longer duration of cooling. Thus, due to this change law in its mineralogical characteristics, exsolved spinel can serve as an important indicator of the original spatial positions of orebodies.

5.2 Laws governing compositions

5.2.1 Compositional zonation

The elemental results from surface scanning show more concentrated Mg and Al in the main body of the exsolved grain, gradually becoming more sparse towards the rim, reflecting the trend of these elements being gathered from the magnetite to the exsolved phase (Fig. 6). The electron microprobe analysis, meanwhile, shows that the Mg content increases from the core to the rim, whereas Fe has the opposite tendency (Fig. 7). This transition from the Mg to Fe shows that spinel exsolution occurred through Mg moving into the exsolution area and Fe moving out of it.

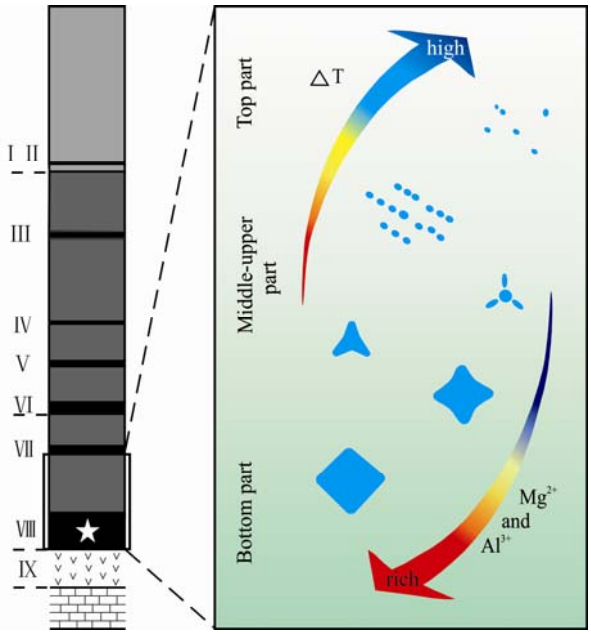

Fig. 8. The pattern diagram of morphological characteristics of spinel from the different part of VIII ore body of the Panzhihua deposit.

The compositional gradient in the primary magnetite solid solution and differences in the thermal history of the Panzhihua intrusion resulted in a clear spatial pattern in the distribution of the abundance, grain size, and morphology of exsolved spinels in different parts of the orebody and intrusion.

According to Equation (1), the rate of diffusion of ions decreases sharply with a decrease in temperature. Furthermore, the diffusion distance(x) is proportional to the square root of time(t):

$$x \propto t^{1/2} \quad (2)$$

As a spinel continues to grow, the diffusion distance increases, and it will take more time for Mg to diffuse to the center of the exsolution feature. As the exsolution interface moves rapidly in a high-temperature environment, the chemical composition of the exsolved phase will not be able to adjust fast enough to remain in equilibrium. This will lead to the rim being preferentially enriched in Mg and a gradual decrease in Mg from rim to center, forming the observed Fe-Mg compositional zonation (Fig. 9). The Fe-Mg compositional zonation went through a long homogenization process and may originally have been more pronounced.

5.2.2 Laws governing Mg#

According to Oswald's law, where more than two phases that are more stable than the existing phase have the potential to form, the most unstable phase will form first and will transform into a more stable phase subsequently (Zhang Youxue, 2006). Based on the analysis herein, magnetite transformed into spinel through a gradual, three-stage process from an exsolution area to a transition phase to an exsolution phase, with a more stable phase forming at every stage. This process is similar to that by which alloyed solid solutions precipitate (Liu Zongchang et al., 2010).

Over the entire course of the exsolution process, an area of the magnetite phase gradually transforms into the spinel phase. Initially, the exsolution area still consists of the magnetite phase, similar to the Guinier-Preston zone of an

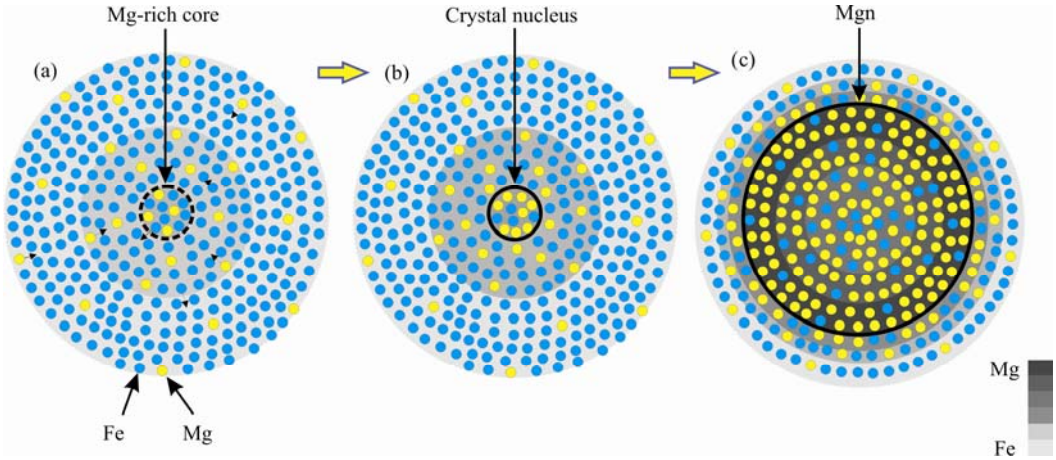

Fig. 9. Schematic diagram of the exsolution and growth of spinel exsolution.

(a), The transformation between Mg and Fe during cooling resulted in some areas enriched with Mg; (b), the area enriched with Mg form into spinel nucleus with the constant enrich of Mg; (c), the chemical composition of spinel exsolution can not adjust timely with the distance of diffusion increases, Mg preferentially enrich at the rim of the exsolution and decrease gradually from the rim to the center forming the Fe-Mg compositional zonation.

alloyed solid solution with a small amount of solute. Through the sustained accumulation of solute, it transforms into the spinel phase. Cation activity is strong, and Mg and Fe maintain a high level of mutual solubility in the high-temperature environment (Wang Pu, 1982); therefore, the exsolution is not only comprised of Mg and Al but also contains Fe. Spinels will contain fewer Fe cations with a decrease in temperature. The exsolved spinels are not stable and will be homogenized by the interdiffusion of Fe and Mg due to the difference between the chemical potential of these components within the particles (Zhang YouXue, 2006). According to Equation (2), smaller exsolved spinels will have a higher degree of homogenization than coarser grains due to the shorter diffusion distance.

Thus, by the processes discussed above, the different exsolution sequences and temperatures plus variation in compositional homogenization led to exsolved spinels of different sizes having a different Fe content (Fig. 10). The coarser-grained spinels, which exsolved earlier, have a lower $Mg^{\#}$ value and steeper Fe-Mg compositional zonation. Thus, Fe-Mg compositional zonation is a record of the exsolution process, showing that the orebody experienced a slow cooling history. Quantitative calculations of the dynamics of Fe^{2+}/Fe^{3+} content in spinel exsolution may offer a new way to calculate the time and temperature of the spinel exsolution process.

6 Conclusions

(1) Spinel exsolution in the Panzhihua Fe-Ti oxide deposit has a magnesia-alumina spinel composition.

(2) Fe-Mg compositional zonation records rapid growth of exsolved grains and shows that the orebody experienced a slow cooling history.

(3) Differences in the exsolution sequence, the temperature at which it occurred, and the degree of compositional homogenization led to variation in the Mg# of exsolved spinels of different grain sizes.

(4) The fractional crystallization of ferrotitanium magma with a high oxygen fugacity in a shallow magma chamber led to compositional differences in the primary magnetite solid solution in different parts of the Panzhihua intrusion. Additionally, different parts of the magnetite solid solution had different thermal histories during cooling. These factors led to differences in spinel growth, resulting in clear spatial patterns in the abundance, grain size, and morphology of spinels within the orebody and intrusion.

(5) Due to the change laws governing its mineralogical characteristics, exsolved spinel has significant utility as a petrogenetic tool to estimate the metallogenetic environment and thermal evolution of the deposit and to judge the original spatial positions of orebodies. For example, coarser-grained exsolved spinels with more complex morphology indicate that the ore body containing them had a lower cooling rate and a longer duration of cooling.

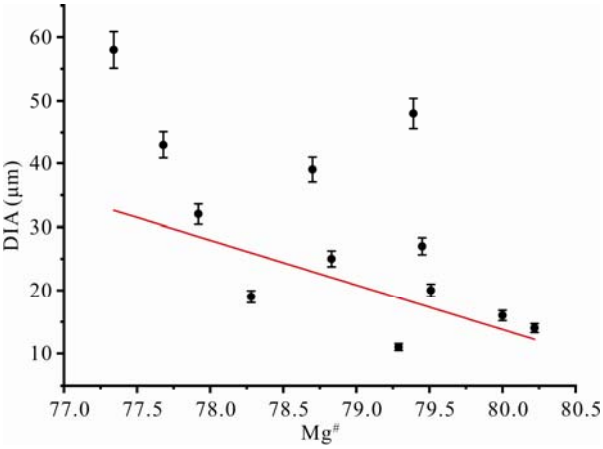

Fig. 10. Variation in $Mg^{\#}$ vs. DIA (diameter) .

Acknowledgments

This work is funded by the National Natural Science Foundation of China (Grant No. 41172047), the Open Fund of the Key Laboratory of Ore Deposit Geochemistry (Institute of Geochemistry, Chinese Academy of Sciences, Guiyang), (Grant No.201308), and the Open Fund of the Key Laboratory Metallogeny and Mineral Resource Assessment, Ministry of Land and Resources (Institute of Mineral Resources, Chinese Academy of Geological Sciences, Beijing) (Grant No. ZS1407). We thank Yandong Peng for helping with the field investigation. We greatly appreciate the detailed reviews of two anonymous reviewers.

Manuscript received Apr. 25, 2017
accepted Dec. 27, 2017
edited by Fei Hongcai

References

Adachi, T., Hokada ,T., Osanai ,Y., Toyoshima, T., Baba ,S., and Nakano, N., 2010. Titanium behavior in quartz during retrograde hydration: Occurrence of rutile exsolution and implications for metamorphic processes in the Sør Rondane Mountains, East Antarctica. *Polar Science*, 3(4): 222–234.

Ahmed, A.H., Arai, S., Abdel-Aziz, Y.M., and Rahimi, A., 2005. Spinel composition as a petrogenetic indicator of the mantle section in the Neoproterozoic Bou Azzer ophiolite, Anti-Atlas, Morocco. *Precambrian Research*, 138: 225–234.

Airiyants, E.V., Zhmodik, S.M., Ivanov, P.O., Belyanin, D.K., and Agafonov, L.V., 2014. Mineral inclusions in Fe-Pt solid solution from the alluvial ore occurrences of the Anabar basin

(northeastern Siberian Platform). *Russian Geology and Geophysics*, 55: 945–958.

Ai Yu, Zhang Zhaochong, Wang Fusheng, Hao Yanli, Zhao Li and Yang Tiezheng, 2006. Trace element and Sr—Nd—Pb—O isotopic system s of the Panzhihua layered gabbro intrusion: constraints on the mantle source regions and origin of V—Ti—Fe oxide deposit. *Acta Geologica Sinica*, (07): 995–1004 (in Chinese with English abstract)

Barnes, S.J., and Roeder, P.L., 2001. The range of spinel compositions in terrestrial mafic and ultramafic rocks. *Journal of Petrology*, 42(12): 2279–2302.

Carswell, D.A., 1980. Mantle derived iherzolite nodules associated with kimberlite, carbonatite and basalt magmatism: a review. *Lithos*, 13(2): 121–138.

Dare, S.A.S., Barnes, S.J., and Beaudoin, G., 2012. Variation in trace element content of magnetite crystallized from a fractionating sulfide liquid, Sudbury, Canada: implications for provenance discrimination. *Geochimica et Cosmochimic Acta*, 88: 27–50.

El Dien, H.G., Morishita, T., Hamdy, M., El-Ela, A.S.A., Hassan, A., and Soda, Y., 2016. Chemical variation of chromian spinel compositions in a serpentinized peridotites: implications for evolution of the Neoproterozoic ophiolites. *Acta Geologica Sinica* (English Edition), 90(1): 210.

Ghiorso , M.S., and Evans, B.W., 2008. Thermodynamics of rhombohedral oxide solid solutions and a revision of the Fe-Ti two-oxide geothermometer and oxygen-barometer. *American Journal of Science*, 308(9): 957–1039.

Guo Guolin, Fan Xiujun, Yang Jingsui, Liu Xiaodong, Zhang Yong and Zhou Wenting, 2015. Petrogenesis significance of chromian spinels from northeastern Jiangxi Province Ophiolite (NEJXO), China: paleogeodynamic implications. *Acta Geologica Sinica* (English Edition), (S2): 18–19.

Guo Guolin, Xu Xiangzhen and Li Jinyang, 2011. The character and genesis of anorthite as inclusions in spinel of mantle peridotites from the Purang ophiolite (southwestern Tibetan Plateau). *Acta Petrologica Sinica*, 11: 3197–3206 (in Chinese with English abstract).

He Detao, Liu Yongsheng, Tong Xirun, Zong Keqing, Hu Zhaochu and Gao Shan, 2013. Multiple exsolutions in a rare clinopyroxene megacryst from the Hannuoba basalt, North China: implications for subducted slab-related crustal thickening and recycling. *Lithos*, 177: 136–147.

Hou Tong, Zhang Zhaochong, Ye Xianren, Encarnacion, J., and Reichow, M.K., 2011. Noble gas isotopic systematics of Fe-Ti -V oxide ore-related mafic-ultramafic layered intrusions in the Panxi area, China: The role of recycled oceanic crust in their petrogenesis. *Geochimica et Cosmochimica Acta*, 75: 6727–6741.

Hou Tong, Zhang Zhaochong and Pirajno, F., 2012. A new metallogenic model of the Panzhihua giant V-Ti-iron oxide deposit (Emeishan Large Igneous Province) based on high-Mg olivine-bearing wehrlite and new field evidence. *International Geology Review*, 54(15): 1721–1745.

Hou Tong, Zhang Zhongchong, Encarnacion, J., Santosh, M., and Sun,Y., 2013. The role recycled oceanic crust in magmatism and metallogenesis:Os-Sr-Nd isotpes, U-b geochronology and geochemistry of picritic dykes in the Panzhihua giant Fe Ti oxide deposit,central Emeishan large igneous province. *Contributions to Mineralogy and Petrology*, 165 (4): 805–822.

Hou Zengqian, Lu Jiren and Lin Shengzhong, 2005. The axial zone consisting of pyrolite and eclogite in the Emei Mantle Plume: major, trace element and Sr-Nd-Pb Isotope evidence. *Acta Geologica Sinica*, (02): 200–219 (in Chinese with English abstract).

Howarth, G.H., Prevec, S.A., and Zhou Meifu, 2013. Timing of Ti-magnetite crystallisation and silicate disequilibrium in the Panzhihua mafic layered intrusion: implications for ore-forming processes. *Lithos*, 170–171: 73–89.

Hu Hao, Li Jianwei, Lentz, D., Ren Zhe, Zhao Xinfu, Deng Xiaodong and Hall, D., 2014. Dissolution-reprecipitation process of magnetite from the Chengchao iron deposit:Insights into ore genesis and implication for in-situ chemical analysis of magnetite. *Ore Geology Reviews*, 57: 393–405.

Irvine, T.N., 1967. Chromian spinel as a petrogenetic indicator part 2: petrologic applications. *Canadian Journal of Earth Sciences*, 4: 71–103.

Karipi, S., Tsikouras, B., Hatzipanagiotou, K., and Grammatikopoulos, T.A., 2007. Petrogenetic significance of spinel-group minerals from the ultramafic rocks of Iti and Kallidromon ophiolites (Central Greece). *Lithos*, 99: 136–149.

Li Wenchen, 1992. The geological characteristics and genesis of Panzhihua Fe-Ti-V Oxide Deposits. *Geology and Prospectin*, 10:20–23 (in Chinese).

Liu Zhao and Tong Laixi, 2015. The petrogenetic link between the Late Paleozoic high-temperature metamorphism in the Altayorogen and the Tarim mantle plume: Evidence from metapelitic and mafic granulites. *Acta Petrologica Sinica*, 06:1761–1773 (in Chinese with English abstract).

Liu Pingping, Zhou Meifu, Chen, W.T., Gao Jianfeng and Huang Xiaowen, 2015. In-situ LA-ICP-MS trace elemental analyses of magnetite: Fe–Ti–(V) oxide-bearing mafic–ultramafic layered intrusions of the Emeishan Large Igneous Province, SW China. *Ore Geology Reviews*, 65: 853–871.

Liu Zongchang, Yuan Zexi and Liu Yongchang, 2010. *Phase transformations in metals and alloys*. Beijing: China Machine Press, 229–232 (in Chinese).

Lo Chinghua, Chung Sunlin, Lee Tungyi and Wu Genyao, 2002. Age of the Emeishan flood magmatism and relations to Permian-Triassic boundary events. *Earth and Planetary Science Letters*, 198: 449–458.

Nadoll, P., Mauk, J.L., Hayes, T.S., Koenig, A.E., and Box, S.E., 2012. Geochemistry of magnetite from hydrothermal ore deposits and host rock of the Mesoproterozoic belt supergroup, United States. *Economic Geology*, 107(6): 1275–1292.

Niu Xiaolu, Yang Jingsui, Liu Fei, Feng Guangying, Tian Yazhou, Zhang Lan, Gao Jian and Zhao Yijue, 2015. Mineralgical and geochemical constraints on the origin of the ultramafic rocks from Wuwamen ophiolite at the southern margin of middle Tianshan, Xingjiang. *Acta Geologica Sinica* (English Edition), 89(2): 70–71.

Pang Kwannang, Zhou Meifu., Lindsley, D., Zhao Donggao, and Malpas, J., 2008. Origin of Fe-Ti oxide ores in mafic intrusions: evidence from the Panzhihua intrusion, SW China. *Journal of Petrology*, 49(2): 295–313.

Pang Kwannang, Li Chusi, Zhou Meifu, and Ripley, E.M., 2009. Mineral compositional constraints on petrogenesis and oxide ore genesis of the late Permian Panzhihua layered gabbroic intrusion, SW China. *Lithos*, 110(1–4): 199–214.

Price, G.D., 1981. Subsolidus phase relations in the titanomagnetite solid solution series. *American Mineralogist*, 66: 751–758.

Rajesh, H.M., 2006. Progressive or continual exsolution in pyroxenes: an indicator of polybaric igneous crystallization for the Perinthatta anorthositic gabbro, northern Kerala, southwestern India. *Journal of Asian Earth Sciences*, 26(5): 541–553.

Righter, K., Keller, L.P., Rahman, Z., and Christoffersen, R., 2012. Exsolution of iron-titanium oxides in magnetite in Miller Range (MIL) 03346 nakhlite: Evidence for post crystallization reduction in the nakhlite cumulate pile. *American Mineralogist*, 99: 2313–2319.

Sautter, V., Haggerty, S.E., and Field, S., 1991. Ultradeep (>300 km) ultramafic xenoliths: Petrological evidence from the transition zone. *Science*, 252: 827–830.

She Yuwei, Song Xieyan, Yu Songyue, Chen Liemeng, Wei Yu and Zheng Wenqin, 2014. The compositions of magnetite and ilmenite of the Taihe layered intrusion, Sichuan Province: Constraints on the formation of the P-rich Fe-Ti oxide ores. *Acta Petrologica Sinica*, (05): 1443–1456 (in Chinese with English abstract).

Shimazaki, H., 1998. On the occurrence of silician magnetites. *Resource Ceology*, 48(1): 23–29.

Song Xieyan, Wang Yulan, Zhang Zhengjie and Ma Runzeng, 1999. Quantitative simulation of formation of the rhythmic layering in layered intrusions—a case study of the Panzhihua layered intrusion, Sichuan. *Acta Geologica Sinica*, (01): 37–46 (in Chinese with English abstract).

Song Xieyan, Hou Zengqian, Cao Zhimin, Lu Jiren, Wang Yunliang, Zhang Chengjiang and Li Youguo, 2001. Geochemical Characteristics and Period of the Emei Igneous Province. *Acta Geologcia Sinica*, 75(4): 498–506 (in Chinese with English abstract).

Song Xieyan, Qi Huawei, Hu Ruizhong, Chen Liemeng and Yu Songyue, 2013. Formation of thick stratiform Fe-Ti oxide layers in layered intrusion and frequent replenishment of fractionated mafic magma: evidence from the Panzhihua intrusion, SW China. *Geochemistry Geophysics Geosystems*, 14(3), 712–732.

Sun Xiaoming, Tang Qian, Sun Weidong, Xu Li, Zhai Wei, Liang Jinlong, Liang Yeheng, Shen Kun, Zhang Zeming, Zhou Bing and Wang Fangyue, 2007. Monazite, iron oxide and barite exsolutions in apatite aggregates from CCSD drillhole eclogites and their geological implications. *Geochimica et Cosmochimica Acta*, 71(11): 2896–2905.

Taghipour, B., and Ahmadnejad, F., 2018. Platinum–group elements geochemistry and chromian spinel composition in podiform chromitites and associated peridotites from the cheshmeh–bid deposit, Neyriz, southern Iran: implications for geotectonic setting. *Acta Geologica Sinica* (English Edition), 92(1), 183–209.

Wang Haipeng, Pring, A., Ngothai, Y., and O'Neill, B., 2005. A low-temperature kinetic study of the exsolution of pentlandite from the monosulfide solid solution using a refined Avrami method. *Geochimica et Cosmochimica Acta*, 69(2): 415–425.

Wang Pu, Pan Yaolu and Weng Lingbao, 1982. *Systematic Mineralogy*. Beijing: Geological Publishing House, 488–489 (in Chinese).

Wang Shixia, Zhu Xiangkun, Song Xieyan and Chen Liemeng, 2012. Fe isotopic characteristics of V-Ti magnetite deposit in Panzhihua area of Sichuan Province and their genetic implications. *Acta Geoscientica Sinica*, 33(6): 995–1004 (in Chinese with English abstract).

Wang Yanguo, Ye Hengqiang and Guo Kexin, 1990. A hrem study of the exsolution and defects in magnetite. *Acta Mineralogica Sinica*, 10(1): 8–14 (in Chinese with English abstract).

Xia Bin, Liu Weiliang, Zhou Guoqing, Wei Zhenquan, Wang Ran, Li Jianfeng, Zhou Yun and Hu Xichong, 2013. Exsolutions in a magnesian eclogite and the geologic significance from western Penh Lake, Tibet. *Journal of Nanjing University(Natural Sciences)*, 03: 356–386 (in Chinese with English abstract).

Xiong Fahui, Yang Jingsui, Paul, R.T., Yildirim, D., Chen Yanhong, Xu Xiangzhen, Liu Zhao, Tian Yazhou, Zhou Wenda, Lai Shengming Zhang Lan, 2015. Diopside and magnetite exsolutions in olivine from Lower Cr# dunite in the Dongbo ophiolite, southern Tibet. *Acta Geologica Sinica* (English Edition), 89(2): 101.

Xiong Fahui, Yang Jingsui, Ba Dengzhu, Gao Jian, Lai Shengming and Zhang Lan, 2016. The feature and tectonic setting of chromitite from the jiesha ophiolite in the eastern yarlung-zangbo suture zone in tibet. *Acta Geologica Sinica*, (11): 3099–3113 (in Chinese with English abstract).

Xu Haijun, Zhang Junfeng, Zong Keqing and Liu Liang, 2015. Quartz exsolution topotaxy in clinopyroxene from the UHP eclogite of Weihai, China. *Lithos*, 226: 17–30.

Yamamoto, S., Komiya, T., Hirose, K., and Maruyama, S., 2009. Coesite and clinopyroxene exsolution lamellae in chromites: In-situ ultrahigh-pressure evidence from podiform chromitites in the Luobusa ophiolite, southern Tibet. *Lithos*, 109(3–4): 314–322.

Yuguchi, T., and Nishiyama, T., 2007. Cooling process of a granitic body deduced from the extents of exsolution and deuteric sub-solidus reactions: Case study of the Okueyama granitic body, Kyushu, Japan. *Lithos*, 97(3–4): 395–421.

Zeng Linggao, Zhang Jun, Sun Teng and Guo Baodong, 2013. Zircon U-Pb age of mafic-ultramafic rock from region in southern Sichuan and its geological implications. *Earth Science (Journal of China University of Geosciences)*, 38(6): 1197–1213 (in Chinese with English abstract).

Zhang Cong, Tian Zuolin, Liu Xiaoyu, Li Peng and Yang Jingsui, 2016. The garnet exsolution texture and petrological investigation on typical pelitic granulite from eastern Himalaya syntaxis. *Acta Geologica Sinica* (English Edition), 90(1): 250–251.

Zhang Youxue, 2006. *Geochemical Kinetics*. Beijing: Higher Education Press, 142–303.

Zhang Zhaochong, Mahoney John J., Mao Jingwen and Wang Fusheng, 2006. Geochemistry of picritic and associated basalt flows of the western Emeishan flood basalt province, China. *Journal of Petrology*, 47(10): 1997–2019.

Zhang Zhaochong, Mao Jingwen, Saunders Andrew D., Ai Yu, Li Ying and Zhao Li, 2009. Petrogenetic modeling of three mafic -ultramafic layered intrusions in the Emeishan large igneous province, SW China, based on isotopic and bulk chemical constraints. *Lithos*, 113(3–4): 369–392

Zhang Xiaoqi, Zhang Jiafei, Song Xieyan, Deng Yufeng, Guan Jianxiang and Zheng Wenqin, 2011. Implications of compositions of plagioclase and olivine on the formation of the Panzhihua V-Ti magnetite deposit, Sichuan Province. *Acta*

Petrologica Sinica, 27(12): 3675–3688 (in Chinese with English abstract).

Zhang Zhibin, Huang Fei, Liu Kaijun, Peng Yandong and Ren Yaqun, 2018. The sequence and genetic mechanism of nano-micron spinel exsolution from Panzhihua V-Ti titanomagnetite deposit. *Earth Siencece*, 43(5):1635–1649 (in Chinese with English abstract).

Zheng Wenqin, Deng Yufeng, Song Xieyan, Chen Liemeng, Yu Songyue, Zhou Guofu, Liu Shirong and Xiang Jianxin, 2014. Composition and genetic significance of the ilmenite of the Panzhihua intrusion. *Acta Petrologica Sinica*, 05:1432–1442 (in Chinese with English abstract).

Zhong Hong and Zhu Weiguang, 2006. Geochronology of layered mafic intrusions from the Pan Xi area in the Emeishan large igneous province, SW China. *Mineralium Deposita*, 41 (6): 599–606.

Zhou Meifu, Malpas, J., Song Xieyan, Robinson, P.T., Sun Min, Kennedy, A.K., Lesher, C.M., and Keays, R.R., 2002. A temporal link between the Emeishan large igneous province (SW China) and the end-Guadalupian mass extinction. *Earth and Planetary Science Letters*, 196(3–4): 113–122.

Zhu Yongfeng and Massonne, H.J., 2007. Pyrrhotite exsoluiton texture of apatite in the mian borehole of the Chinese Continental Sceientific Dirlling (CCSD). *Acta Petrologica Sinica*, 23(12): 3249–3254 (in Chinese with English abstract).

Zhu Yongfeng and Xu Xin, 2007. Exsolution texture of two-pyroxenes in lherzolite from Baijiangtan opiolitic mélange, western Junggar, China. *Acta Petrologica Sinica*, 23(5): 1075–1086 (in Chinese with English abstract).

About the first author

ZHANG Zhibin was born in 1990. He obtained his Bachelor's degree in 2014 and Master's degree in 2017 from Northeastern University, China. He is still studying for his Ph.D. in School of Resources and Civil Engineering, Northeastern University, China. His research interests are focused on exsolution microstructures in Fe–Ti oxides and sulfides and mineralogy in mafic and ultramafic layered intrusions. Tel: 86-15998388952. E-mail: zzbin0502 @163.com.